Arabian Journal of Chemistry (2023) **16**, 104959

King Saud University

Arabian Journal of Chemistry

www.ksu.edu.sa
www.sciencedirect.com

ORIGINAL ARTICLE

Utilization of agricultural waste to herbicide removal: Magnetic BEA zeolite adsorbents prepared by dry-gel conversion using rice husk ash–derived SiO_2 for paraquat removal

Vanpaseuth Phouthavong [a], Takeshi Hagio [a,b,*], Jae-Hyeok Park [b], Supinya Nijpanich [c], Teeranun Srihirunthanon [d,e], Nutchanan Chantanurak [d,e], Kanchanok Duangkhai [d,e], Ratana Rujiravanit [d,e], Vanseng Chounlamany [f], Kesiny Phomkeona [f], Long Kong [g], Liang Li [g], Ryoichi Ichino [a,b]

[a] *Department of Chemical Systems Engineering, Graduate School of Engineering, Nagoya University, Furo-cho, Chikusa-ku, Nagoya 464-8603, Japan*
[b] *Institute of Materials Innovation, Institutes of Innovation for Future Society, Nagoya University, Furo-cho, Chikusa-ku, Nagoya 464-8601, Japan*
[c] *Synchrotron Light Research Institute (Public Organization), Nakhon Ratchasima 30000, Thailand*
[d] *The Petroleum and Petrochemical College, Chulalongkorn University, Bangkok 10330, Thailand*
[e] *Center of Excellence on Petrochemical and Materials Technology, Chulalongkorn University, Bangkok 10330, Thailand*
[f] *Department of Chemistry, Faculty of Natural Sciences, National University of Laos, Vientiane Capital, Laos*
[g] *School of Environmental Science and Engineering, Shanghai Jiao Tong University, 800 Dongchuan Road, Shanghai 200240, China*

Received 31 January 2023; accepted 25 April 2023
Available online 2 May 2023

KEYWORDS

Herbicide removal;
Paraquat;
Magnetic BEA zeolite;
Rice husk ash;
Dry-gel conversion

Abstract This study presents a method that will allow for the sustainable utilization of rice husk ash-SiO_2 (RHAS), an agricultural-waste–derived material, as a bulky solid SiO_2 source in the zeolite beta (BEA)/Fe_3O_4 composite (magnetic RHAS-BEA) synthesis via a dry-gel conversion method for the removal of paraquat, a typical herbicide, from aqueous solutions. Ultrasonic waves were used to facilitate the formation of uniform Fe_3O_4-contained dry precursor gel before converting to the magnetic BEA zeolite composite for the first time. Magnetic RHAS-BEA was then characterized and

* Corresponding author at: Institute of Materials Innovation, Institutes of Innovation for Future Society, Nagoya University, Furo-cho, Chikusa-ku, Nagoya 464-8601, Japan.
E-mail address: hagio@mirai.nagoya-u.ac.jp (T. Hagio).
Peer review under responsibility of King Saud University.

Production and hosting by Elsevier

https://doi.org/10.1016/j.arabjc.2023.104959

compared with a non-magnetic sample (RHAS-BEA) using X-ray diffraction and field-emission scanning electron microscopy. In terms of adsorption, we found that paraquat had a high adsorption rate on the samples and conformed to a pseudo-second-order kinetic model. The adsorption behavior of paraquat on the synthesized RHAS-BEA and magnetic RHAS-BEA obeyed the Langmuir adsorption isotherm model. The synthesized adsorbents were reusable for at least four cycles, via thermal regeneration at 450 °C. The inclusion of Fe_3O_4 particles in magnetic RHAS-BEA disrupted neither the crystallization of the BEA zeolite nor the adsorption of paraquat and enabled easy collection via an external magnet.

1. Introduction

Paraquat, one of the many commercial names of 1,1′-dimethyl-4,4′-b ipyridinium dichloride, is a widely used bipyridyl herbicide because of its non-selectivity and cost-effectiveness. However, paraquat has been banned in several countries due to its deleterious effects on the health of a variety of organisms (including humans). Specifically, chronic exposure to this chemical can damage various organ systems, tissues, and cells (including kidney, liver, and neurons), culminating in a wide-range of cancers (such as skin, brain, and breast); in severe cases, it can eventually result in death (Huang et al., 2019b; Kouchakinejad et al., 2022). Agricultural areas in which paraquat is used excessively are characterized by an accumulation of paraquat residues in the soil. Owing to their high solubility, these residues migrate to groundwater and surface water, damaging the ecological integrity of various habitats and negatively impacting human and animal health (Fernandes et al., 2017). In previous studies, paraquat contamination in soil was found in the range of 0.1525–14.4366 mg/kg in Indonesia (Ardiwinata et al., 2021), whereas the contamination level in the surface water of Thailand and Spain was 1.5–18.9 and 3.95–87 μg/L, respectively, and that in groundwater in Thailand was 1.5–18.9 μg/L (Franco et al., 2022). To address these environmental and health concerns, methods that will facilitate the removal of paraquat from water must be developed.

Adsorption is an effective physical approach for treating water contaminated with pesticides and other organic pollutants. To date, various adsorbents with diverse structures, porosities, and pore and particle sizes have been developed to specifically target certain pollutants (Saleh et al., 2020). Several adsorbents have been developed and applied for the removal of paraquat from water; these adsorbents include clays, zeolites, mesoporous SiO_2, graphene oxide, activated carbon, and biopolymers. These materials have recently been summarized in a review article (Franco et al., 2022) and have shown good adsorption, ranging from a few milligrams to hundreds of milligrams of paraquat per gram of adsorbent. However, sustainable and environmentally friendly adsorbents for herbicide removal are yet to be developed. Synthetic zeolites, a group of microporous crystalline aluminosilicate compounds consisting of $SiO_{4/2}$ and negatively charged $[AlO_{4/2}]^-$ tetrahedra, are of special interest because of their unique adsorption properties stemming from their uniformly sized pores and tunable hydrophobicity/hydrophilicity, which can be controlled by adjusting the Si/Al ratio and synthesis conditions. Porous frameworks with large surface areas and negatively charged Al sites make zeolites outstanding adsorbents and cation exchangers for capturing organic compounds and cations. Specifically, zeolite beta (BEA) is one of the most widely used zeolites because of its large three-dimensional pore system (pore size: 0.76 × 0.64 and 0.55 × 0.55 nm), high thermal stability, and acidity (Bok et al., 2020). Therefore, it is a good candidate for the environmentally friendly removal of paraquat (Rongchapo et al., 2013).

Furthermore, composites of zeolites and magnetic particles facilitate easy collection after use by attracting the composite particles to a magnet (Loiola et al., 2022). Zeolite/magnetic material composites are commonly synthesized by crystallizing zeolites in the liquid phase in the presence of magnetic particles via conventional hydrothermal synthesis. However, the incorporation of magnetic particles into zeolite crystals is not ensured because the crystallization of zeolite cannot be controlled to occur in the vicinity of magnetic particles; instead, it occurs in randomly in a solution. To address this issue, our research group recently proposed and succeeded in synthesizing a BEA-type zeolite/magnetite (Fe_3O_4) composite via dry-gel conversion (DGC) for the first time (Phouthavong et al., 2020). In the DGC method, a uniform dry gel containing well-dispersed magnetic particles is prepared by drying a magnetic-particle-suspended zeolite precursor solution that is crystallized into zeolite using high-pressure hot water vapor in a sealed autoclave. The high uniformity of the gel resulted in a zeolite product with a uniform and good incorporation of magnetic particles. Moreover, the incorporation of magnetic particles had no effect on the crystallinity of the BEA zeolite, which showed high cationic dye adsorption performance and magnetic separability. The DGC method has several advantages, which are as follows: a lower reactor volume, high conversion rate (high yield), and less waste generation because no washing is required during the collection of the product.

Asian countries such as China, India, Indonesia, Bangladesh, Vietnam, Thailand, Myanmar, the Philippines, and Japan produced over 80 to 1.5 of billion tons paddy and milled rice in the 2010 s (FAO, 2022), accounting for approximately 90% of the global product share. Therefore, these countries produce a large amount of rice husk (RH) (i.e., agricultural waste). RH can be used as a fuel to generate energy owing to its high heating value (Steven et al., 2021). The ash that is produced after RH is burnt is considered an abundant source of bio-SiO_2, which can be found up to 99 wt% on a dry basis, depending on the conditions under which it is synthesized (Steven et al., 2021). SiO_2 derived from rice husk ash, rice husk ash-SiO_2 (RHAS), mainly exists in a highly reactive amorphous form depending on the extraction conditions and calcination temperature (Santana Costa and Paranhos, 2018). Hence, highly reactive RHAS is a sustainable and inexpensive surrogate SiO_2 source for producing SiO_2-containing materials that are used in broad applications, such as concrete (Shams et al., 2022), catalysis/catalyst supports, drug carriers, and environmental remediation (Gebretatios et al., 2023). Many researchers have successfully utilized RHAS for the preparation of zeolites, such as ZSM-5 (MFI) (Sivalingam and Sen, 2020; Wang et al., 2018), faujasite (FAU) (Rongchapo et al., 2013, 2015; Tolentino et al., 2020; Wang et al., 2018), Linde-type A (Wang et al., 2018), chabazite (CHA) (Flores et al., 2021), analcime (Banerjee et al., 2017), and BEA (Prasetyoko et al., 2006; Rongchapo et al., 2013), using conventional hydrothermal processes carried out in the liquid phase. However, there are no reports on its application in zeolite synthesis using DGC. In a previous study (Phouthavong et al., 2020), we obtained a uniform dry precursor gel using a commercial colloidal form of SiO_2. Therefore, to directly utilize bulky solid RHAS in the DGC method, some modifications to the gel preparation method are necessary. If RHAS is applied to the DGC synthesis of magnetic zeolites, would allow for the creation of a more sustainable and environmentally friendly process. Moreover, it could be applied toward the sustainable extraction of herbicides from the environment.

The aim of this study is to propose an environmentally friendly method for the preparation of magnetic BEA zeolites using the DGC method through a modified gel preparation method involving ultrasonic waves. This will enable the utilization of bulky solid RHAS as a sustainable SiO_2 source. The performance of the synthesized magnetic adsorbent for paraquat adsorption was investigated by determining its adsorption kinetics and the mechanisms underlying its operation. The magnetic separation performance and reusability of the adsorbent after adsorption were evaluated and discussed. This study demonstrates the sustainable recycling of agricultural waste in the remediation of water polluted via agricultural activities.

2. Materials and methods

2.1. Materials

Fe_3O_4 was selected as the magnetic material owing to its environmental friendliness. The following materials were used in the synthesis of the BEA zeolite/Fe_3O_4 composite (magnetic RHAS-BEA). RHAS was extracted from rice husk ash provided by CP All Public Co., Ltd., Thailand, using an alkaline extraction, followed by acid precipitation (see Supplementary Information for details). All other chemicals used in this study were of reagent grade. The Al source, alkali source, structure-directing agent (SDA), and magnetic particles were $Al_2(SO_4)_3 \cdot 16H_2O$ (Nacalai Tesque, Japan), NaOH (Nacalai Tesque, Japan), tetraethyl ammonium hydroxide (TEAOH; 35 wt%, Tokyo Chemical Industry, Co., Ltd., Japan), and Fe_3O_4 (Kanto Chemical, Co., Inc., Japan) with Heywood diameters of primary particles in the range 100–300 nm. To perform the adsorption experiments, paraquat solutions were prepared by dissolving appropriate amounts of paraquat dichloride ($C_{12}H_{14}Cl_2N_2$, Tokyo Chemical Industry, Co., Ltd., Japan) in distilled water (DW). The pH of the solution was adjusted using 0.1 mol/L hydrochloric acid, diluted from concentrate hydrochloric acid (HCl; 36 wt%, Nacalai Tesque, Japan), and 0.1 mol/L NaOH, prepared by dissolving NaOH (Nacalai Tesque, Japan) in DW. A sodium chloride solution (0.01 mol/L) was prepared by dissolving sodium chloride (NaCl; Nacalai Tesque, Japan) in DW and was used to determine the pH at the point of zero charge. Silicon (Si, 1.00 mgSi/mL, Nacalai Tesque, Japan), aluminum (Al, 1002 mg/L, Fujifilm Wako Pure Chemical Corporation, Japan), and iron (Fe, 1001 mg/L, Fujifilm Wako Pure Chemical Corporation, Japan) standard solutions were used in the quantification of leached ions during the adsorption test. Diquat dibromide monohydrate (Fujifilm Wako Pure Chemical Corporation, Japan) and Cibacron blue 3GA (CB, Sigma-Aldrich, USA) were used in the paraquat co-adsorption test.

2.2. Synthesis of magnetic RHAS-BEA

Magnetic RHAS-BEA was synthesized based on a previously reported DGC protocol (Phouthavong et al., 2020) and modified for RHAS utilization (Fig. 1). RHAS (3.63 g) was dissolved in 1.00 g of a 20 wt% NaOH solution (prepared by dissolving NaOH pellets in DW) and 1.033 g of a 10 wt% TEAOH solution (diluted from 35 wt% TEAOH in DW) by employing mechanical stirring for 30 min. Ultrasonication was then applied, using an ultrasonic bath (US-104, SND Co., Ltd., Japan), for 2 h to improve the dispersion and dissolution of RHAS before the addition of 0.30 g of the Al source. Ultrasonication was performed again for 1 h. The mixture was then continuously stirred in a closed container for 16 h before the temperature was increased to 80 °C. After the solution was stirred for 8 h at 80 °C, 1.12 g Fe_3O_4 was introduced to the mixture. For comparison, Fe_3O_4 was excluded when preparing the non-magnetic RHAS-BEA sample (abbreviated as RHAS-BEA hereafter). The container was opened until the precursor solution transformed into a homogeneous and dry precursor gel. The dried gel was collected and crushed before being placed in a small container inside an autoclave. An equivalent weight of water was added to the autoclave without direct contact with the gel. The autoclave was then heated to 180 °C for 12 h in a convection oven (SOFW-300SB, AS ONE Corporation, Japan) to obtain the product, which was easily collected (i.e., it was dry) without washing. The pre-crushed products were calcined in an electric furnace (VF-3000, SK Medical Electronics Co. Ltd., Japan) at 450 °C for 12 h (in air) to remove the SDA before use.

2.3. Characterization

The presence of the BEA zeolite and iron oxides in the samples was analyzed by performing X-ray diffraction (XRD; UltimaIV, Rigaku Corporation, Japan) equipped with a Cu-Kα X-ray source (α = 1.5405 Å). The morphologies of the synthesized samples were observed by applying field-emission scanning electron microscopy (FE-SEM; JSM-6330F, JEOL, Japan). Ultra-high-resolution FE-SEM-energy dispersive X-ray spectroscopy (FE-SEM-EDS; S-4800, HITACHI, Japan) was used to determine the Si/Al ratio of the samples and observe the distribution of the magnetic particles in the magnetic RHAS-BEA sample.

2.4. Paraquat adsorption experiments

2.4.1. Adsorption kinetics and adsorption isotherm

All paraquat adsorption kinetics and isotherm experiments were conducted by adding 1 g/L of the calcined adsorbents to the paraquat solutions, followed by shaking at a constant speed of 120 rpm using an orbital shaker (SK-O180-S, DLAB Scientific Co., Ltd., Beijing, China) at 26 °C. After adsorption, the adsorbents were removed from the solution using PTFE syringe filters (pore size 0.22 μm, Membrane Solutions, Japan). The paraquat concentration in the solutions was quantified using paraquat dichloride reference standard grade for pesticide residue analysis (Fujifilm Wako Pure Chemical Corporation, Japan) and a UV–Vis spectrophotometer (λ = 257 nm; UV-2450, Shimadzu Co., Japan). The amount of paraquat adsorbed per unit mass of adsorbent was calculated as follows:

$$q_e = \frac{(C_0 - C_e)V}{m} \quad (1)$$

where q_e is the amount of adsorbed paraquat per unit mass of the adsorbent at equilibrium (mg/g), C_0 is the initial concentration of paraquat (mg/L), C_e is the equilibrium concentration of paraquat (mg/L), V is the solution volume (L), and m is the mass of the adsorbent (g).

Adsorption kinetics tests of paraquat on the RHAS-BEA and magnetic RHAS-BEA samples were conducted to investigate the effect of time on paraquat adsorption by shaking the adsorbent in a paraquat solution with a fixed concentration of

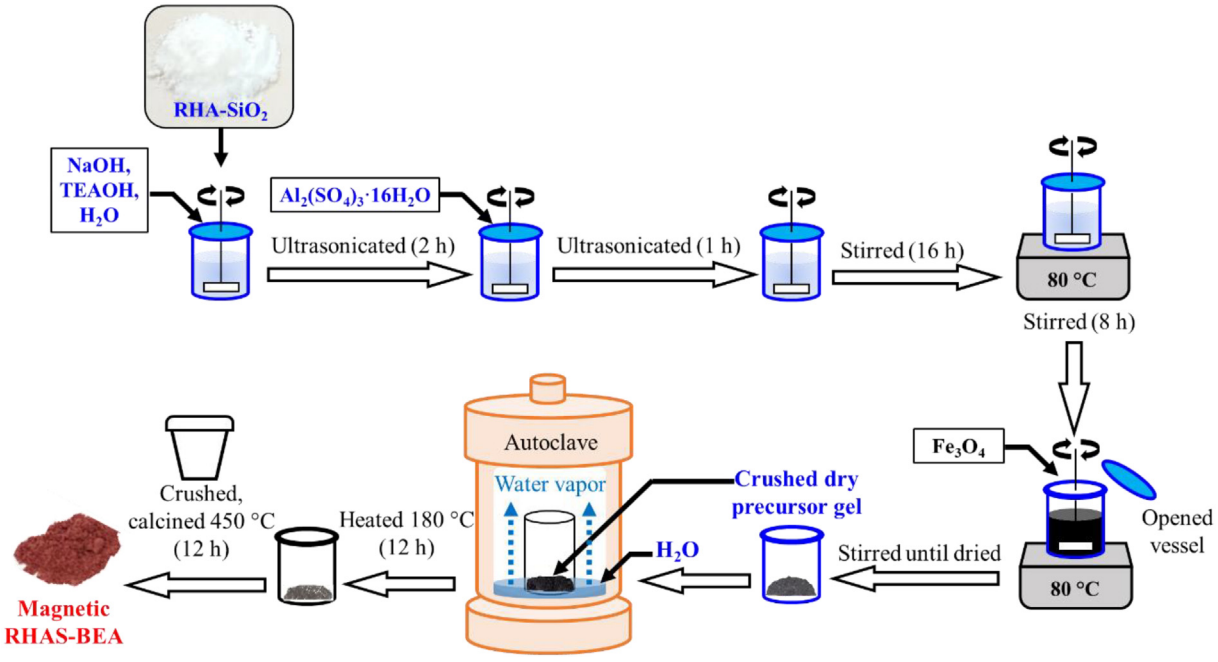

Fig. 1 Synthesis of magnetic RHAS-BEA using DGC method.

75 mg/L for various contact times between 1 and 1440 min. The initial pH value of the paraquat solution was 5.8 (non-adjusted), and the adsorption was performed at 26 °C. The amount of paraquat adsorbed per unit mass of adsorbent at time t (q_t) was calculated using Eq. (1), using the concentration of paraquat at time t (C_t). Linearized adsorption kinetic models, including pseudo-first-order (Eq. (2)), pseudo-second-order (Eq. (3)), and intraparticle diffusion (Eq. (4)) were used to evaluate the paraquat adsorption rate and predict the adsorption mechanism. These are the three most common models used in adsorption studies of organic pollutants on various types of adsorbents (Tan and Hameed, 2017):

$$\ln(q_e\text{-}q_t)=\ln q_e\text{-}k_1 t \quad (2)$$

$$\frac{t}{q_t}=\frac{1}{k_2 q_e^2}+\frac{1}{q_e t} \quad (3)$$

$$q_t = k_{id}\sqrt{t}+C \quad (4)$$

where q_e and q_t are the adsorbed amounts of paraquat per unit mass of the adsorbent at equilibrium (mg/g) and time t (mg/g), respectively; t is the adsorption time (min); k_1, k_2, and k_{id} are the adsorption kinetic constants of the pseudo-first-order (in 1/min), pseudo-second-order (in g/mg min), and intra-particle diffusion (in mg/(g·min$^{1/2}$)) models, respectively; C is the intercept of the intra-particle diffusion model, which proportionally represents the thickness of the boundary layer (Jodeh et al., 2019).

For the adsorption isotherm experiments, the calcined samples were suspended in paraquat solutions prepared at concentrations ranging from 10 to 750 mg/L for 24 h at 26 °C. The solutions were collected to measure C_e and evaluate q_e using Eq. (1). Langmuir and Freundlich adsorption isotherm models were used to evaluate the maximum adsorption capacity and adsorption behavior of paraquat on RHAS-BEA and magnetic RHAS-BEA. The linear forms of each model are as follows:

Langmuir: $\frac{C_e}{q_e}=\frac{C_e}{q_m}+\frac{1}{q_m b}$,

Freundlich: $\log q_e=\frac{1}{n}\log C_e+\log K_F$, where q_m is the maximum adsorbed amount of paraquat per unit mass of the adsorbent (mg/g) obtained from the linearized Langmuir equation, b is the Langmuir constant related to the affinity of paraquat for the adsorbents (L/mg), n is the Freundlich adsorption intensity, and K_F is the Freundlich constant related to the adsorption capacity (mg^{1+n}/g L^n).

2.4.2. Effect of initial pH and determination of the pH values at the point of zero charge

The calcined adsorbents were suspended in paraquat solution with a fixed concentration of 100 mg/L, but the initial pH values were adjusted from 2.8 to 9.3 using 0.1 mol/L HCl or NaOH solutions. The suspension was then shaken for 24 h. The q_e value at each initial pH was calculated using Eq. (1) to evaluate the effect of the initial pH on paraquat adsorption. The pH values at the point of zero charge (pH_{pzc}) of the calcined samples were determined to explain the adsorption mechanism. This was evaluated using the difference between the initial and final pH values of the salt solution series after shaking with the adsorbents (Jiao et al., 2017). A 0.5 g/L suspension of the adsorbents in 0.01 mol/L NaCl solutions with initial pH values (pH_i) in the range of 2.9–10.0 was shaken for 24 h at 26 °C. The final pH (pH_f) was measured after filtration, using a pH meter (AS800, AS ONE Corporation, Japan). The differences between pH_f and pH_i were plotted against their pH_i values. The point at which the connecting line passes through pH = 0 is the pH_{pzc} of the adsorbent.

2.5. Separability of the adsorbents from aqueous solutions

The separability of the adsorbents from the aqueous solutions was examined by monitoring their sedimentation in the absence and presence of magnets (Hagio et al., 2019; Phouthavong et al., 2020). Suspended RHAS-BEA and mag-

netic RHAS-BEA particles at a concentration of 100 mg/L in DW were shaken for 2 h before being allowed to stand in the absence or presence of a neodymium (Nd) magnet (surface flux density of 0.45 T). The turbidity of the supernatant was measured in formazin turbidity units; specifically, the turbidity of the supernatant was consecutively measured for 0.5–60 min using a turbidimeter (HI93703, Hanna Instruments, USA). Suspended solids (SS) (mg/L) at each monitored standing time were calculated from the turbidity values using a calibration curve.

2.6. Reusability of the adsorbents and ions leached from the adsorbents

Spent RHAS-BEA and magnetic RHAS-BEA were collected after one paraquat adsorption test, regenerated by recalcination at 450 °C for 6 h, and reused in subsequent paraquat adsorption cycles. Adsorption and regeneration cycles were repeated to evaluate the reusability. Each adsorption cycle was performed in duplicates. The ions leached from the adsorbents were examined by shaking the adsorbents (1 g/L) in water and paraquat solution (1 mg/L) for 3 h at 26 °C. The solutions were collected to quantify potentially leached elements, such as Si, Al, and Fe, using inductively coupled plasma-atomic emission spectrometry (S-II, Seiko Instrument, Japan).

2.7. Paraquat co-adsorption test with blue dye

The selectivity in the presence of blue dye added to commercial paraquat was tested in practical applications. Aqueous solutions of paraquat (40 μmol/L, equivalent to 10 mg/L) were prepared separately and mixed with CB at two different concentrations (4 and 40 μmol/L). Single and binary adsorption tests were performed using a ratio of 1 g adsorbent per 1 L solution, contact time of 24 h at 26 °C, and the pH values of the solutions were not adjusted. The concentrations of CB and paraquat in the solutions were determined from the absorbances recorded using a UV–Vis spectrophotometer (UV-2450, Shimadzu Co., Japan) at 600 and 257 nm, respectively. The blue dye also showed intense UV absorption at λ_{257nm} which is the analytical detection wavelength of paraquat (Fig. S1). Thus, the co-absorption of CB at λ_{257nm} was subtracted from the absorption of paraquat in the binary mixture using the constant ratio between the absorbance at λ_{257nm} and λ_{600nm} of a single CB.

2.8. Paraquat co-adsorption test with diquat

Aqueous solutions of paraquat (40 μmol/L, equivalent to 10 mg/L) were prepared separately and mixed with diquat at equivalent molarity. The adsorption was performed using 1 g adsorbent per 1 L solution, contact time of 24 h at 26 °C, and the pH values of the solutions were not adjusted (pH 5.8). UV absorption spectra of paraquat and diquat were recorded using the UV–Vis spectrophotometer.

3. Results and discussion

3.1. Characterization of the RHAS-BEA and magnetic RHAS-BEA

The XRD pattern of RHAS (Fig. 2a) has a broad peak, indicative of its highly amorphous structure; additionally, no crystalline phase was detected. The RHAS particles have ultrafine sizes (i.e., they are below 100 nm) (inset of the scanning electron microscopy (SEM) image in Fig. 2a). For synthesizing advanced materials, amorphous SiO_2 is the preferred source of SiO_2 owing to its high reactivity (Santana Costa and Paranhos, 2018; Steven et al., 2021). Prior to the inclusion of the Fe_3O_4 particles, preliminary studies were conducted to confirm the crystallization of BEA zeolites using RHAS via the DGC method. Initially, the precursor gel was prepared by mixing RHAS with an Al source in NaOH and TEAOH solutions, using simple mechanical stirring at room temperature (26 °C). The DGC process primarily produced an amorphous product with a minor crystalline phase at $2\theta = 32.0°$ and 34.0°, which can be classified as a CHA zeolite (Criado et al., 2007; Dang et al., 2020), as indicated by the XRD pattern and the inset SEM image in Fig. 2b. This product may have been brought forth due to the insufficient dissolution of the SiO_2 source for the generation of $SiO_{4/2}$ tetrahedra to form a dense aluminosilicate gel. Therefore, the amount of NaOH, temperature, and aging time were increased to facilitate optimal dissolution. These increases significantly improved the synthesis, as indicated by the characteristic XRD peaks ($2\theta = 7.6°$ and 22.4°) which were congruent with the standard card (JCPDS 48–0074) of BEA zeolite (El Maksod et al., 2017), and some crystals with clear boundary shapes in the inset SEM image in Fig. 2c. Overall, the crystallinity and morphology of the BEA zeolite significantly improved, as shown in Fig. 2d, with the assistance of ultrasonication for the dissolution of RHAS and mixing with the alumina source. The observed XRD peaks agreed well with those of BEA zeolites that were synthesized in other studies using commercial colloidal SiO_2 via the DGC method (Inagaki et al., 2007; Matsukata et al., 2002; Phouthavong et al., 2020). Ultrasonication was used to prepare a dry precursor gel containing Fe_3O_4 particles. The BEA zeolite phase was still detectable in the presence of Fe_3O_4, as observed through XRD (Fig. 2e).

The as-synthesized non-magnetic and magnetic RHAS-BEA samples were calcined at 450 °C for 12 h to remove the SDA and open their pores for paraquat adsorption. The XRD patterns of the calcined products are shown in Fig. 3a and 3b, displaying the characteristic peaks of BEA in both samples. These results confirm that the BEA structure did not collapse after the removal of the SDA through calcination. The XRD peaks in the 2theta range of 30°–40° corresponded to the incorporated Fe_3O_4 (JCPDS 19–0629) in the magnetic sample (Fig. 3b), while that of a small amount of hematite (α-Fe_2O_3, JCPDS 01–1053) was also detected, indicative of the slight oxidation of Fe_3O_4 caused by in-air calcination (Fauzi and Ratnawulan, 2021).

The FE-SEM images in Fig. 4 show the morphologies of the calcined samples. We found that the crystals of both samples predominantly had rectangle-like faces; this is typical of BEA-type zeolites prepared by using the DGC method (Inagaki et al., 2007; Matsukata et al., 2002). SEM observations revealed the presence of aggregates with particle sizes below 1 μm (Fig. 4a). However, the aggregate size of the magnetic RHAS-BEA sample was smaller than that of the non-magnetic RHAS-BEA sample. The presence of Fe_3O_4 particles could have decreased the aggregate size of the product; this could have occurred because of the larger number of nuclei created between the Fe_3O_4 particles in the precursor gel (Hagio et al., 2019; Miao et al., 2022). Additionally, the aggre-

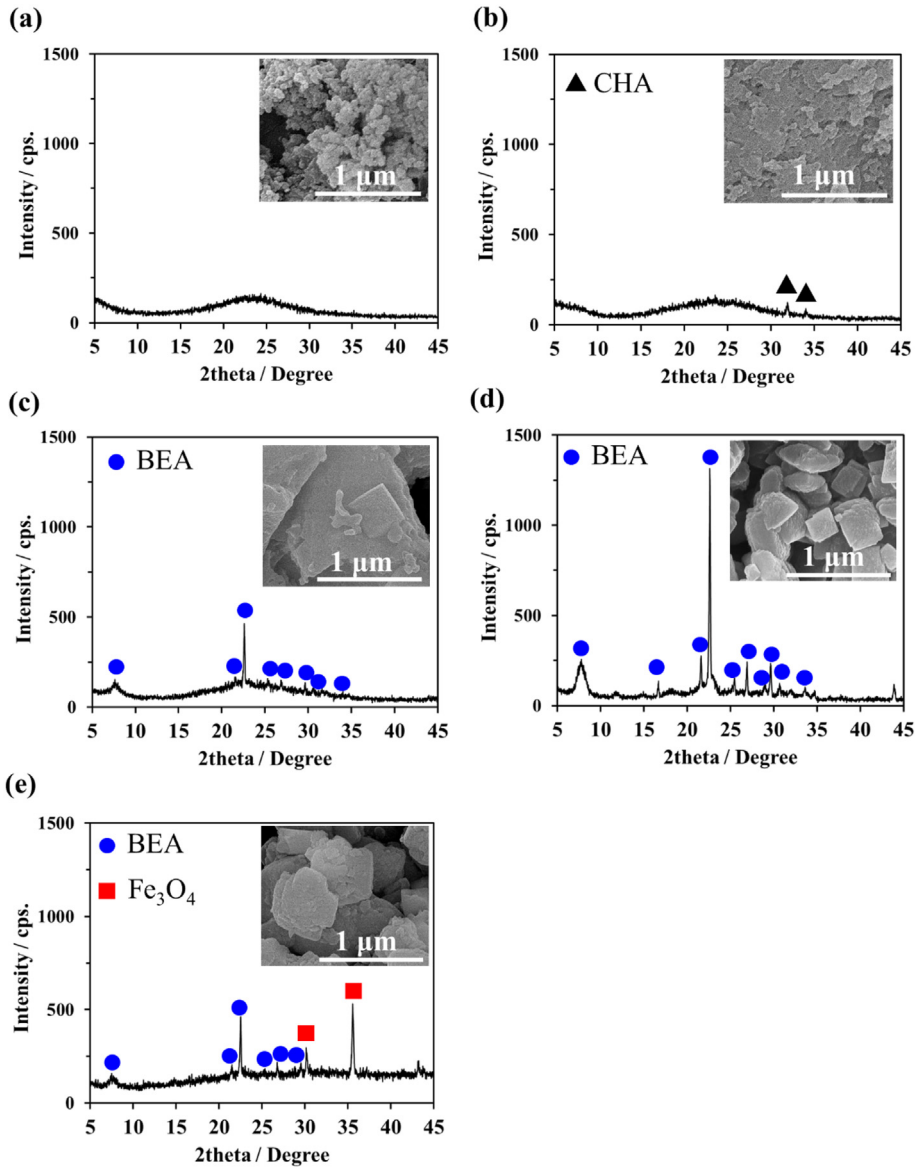

Fig. 2 (a) XRD pattern of RHAS with its inset SEM image, and XRD patterns with their inset SEM images of as-synthesized products using gels prepared at room temperature (b), at 80 °C with increased NaOH (c), at 80 °C with increased NaOH and ultrasonication for non-magnetic (d) and magnetic RHAS-BEA prepared under the same conditions as (d) (e).

gate size distribution of the precursor gel may affect the aggregate size of the crystallized products. Higher-magnification images (Fig. 4b) showed that the samples have rough surfaces, indicative of nanoparticle aggregation (Inagaki et al., 2007). Notably, the incorporation of the Fe_3O_4 particles into the magnetic samples hardly changed the morphology of the BEA zeolite. FE-SEM-EDS elemental mapping revealed that the Si/Al ratios of RHAS-BEA and magnetic RHAS-BEA were 48.8 and 45.0, respectively, and therefore could be classified as high-SiO_2 zeolites (Li et al., 2023). Fig. 5 depicts the distribution of Si and Fe in magnetic RHAS-BEA at almost the same positions; this shows that all BEA particles contain Fe_3O_4 particles. Therefore, these results confirm the success of using amorphous RHAS as the SiO_2 source in the DGC method to crystallize BEA-type zeolites and that the inclusion of Fe_3O_4 particles did not hinder the crystallization of these zeolites.

3.2. Paraquat adsorption studies

In kinetic studies conducted at 26 °C, a significant amount of paraquat was quickly adsorbed on RHAS-BEA and magnetic RHAS-BEA within 1 min in the first stage of contact time (Fig. 6a) and sharply increased within 10 min. This is indicative of the high adsorption rates of the synthesized adsorbents. Subsequently, adsorption slowed and reached saturation at 60 min. Fast adsorption of paraquat has also been reported in previous studies using zeolites such as FAU (Pukcothanung et al., 2018), modified FAU (Nur et al., 2005), and MFI (Walcarius and Mouchotte, 2004). The non-

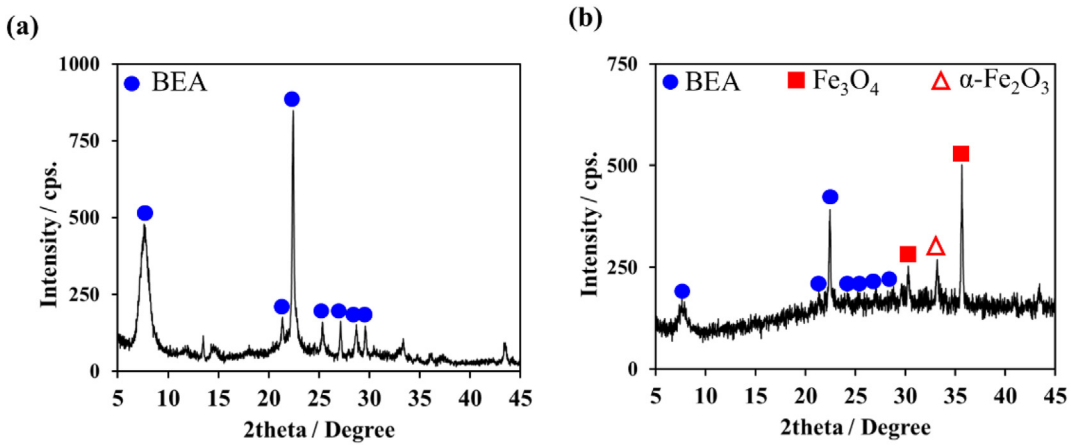

Fig. 3 XRD patterns of (a) RHAS-BEA and (b) magnetic RHAS-BEA samples calcined at 450 °C (12 h).

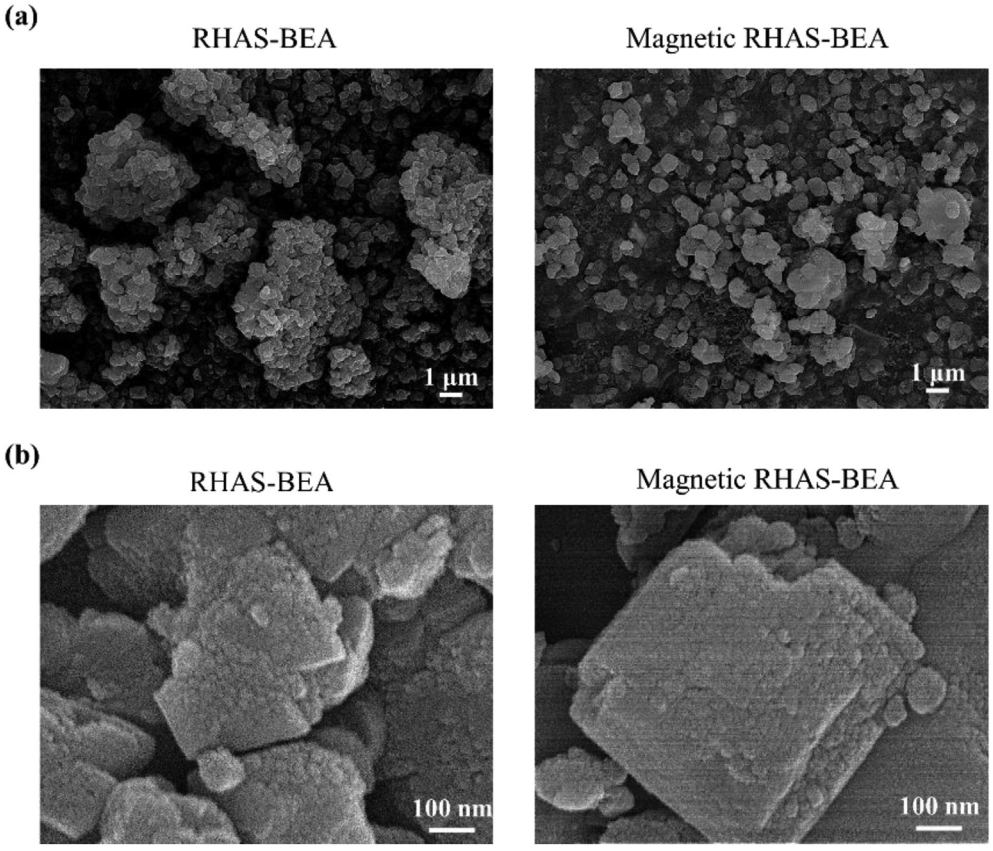

Fig. 4 FE-SEM photomicrograph of RHAS-BEA and magnetic RHAS-BEA samples observed at × 5000 magnification (a) and × 100000 magnification (b).

magnetic and magnetic RHAS-BEA revealed similar adsorption kinetic trends, but the amount of adsorbed paraquat was lower for the magnetic sample. This is likely due to the lower fraction of the adsorbent (i.e., BEA zeolite). These details are discussed in the next paragraph along with an isotherm study. Using widely applied linear adsorption reaction kinetic models, the adsorption of paraquat on both BEA samples best fit the pseudo-second order model according to the coefficient of determination (R^2) shown in Fig. 6b and 6c. This indicates that the surface reaction (i.e., chemisorption) occurred in the electrostatic interaction between paraquat and the adsorbents (Moradi, 2014). Similar pseudo-second-order kinetic constants (k_2) for paraquat adsorption on the RHAS-BEA and magnetic RHAS-BEA samples (i.e., 0.0087 and 0.0078 g/mg min, respectively) revealed that the inclusion of Fe_3O_4 particles in the BEA zeolite had a negligible effect on the paraquat adsorption rate. The intraparticle diffusion model also showed a good fit (Table S1) considering

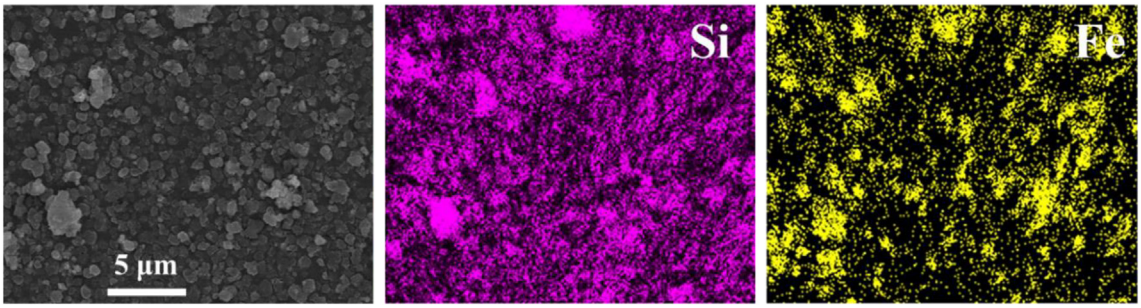

Fig. 5 FE-SEM-EDS elemental mapping of the calcined magnetic RHAS-BEA sample.

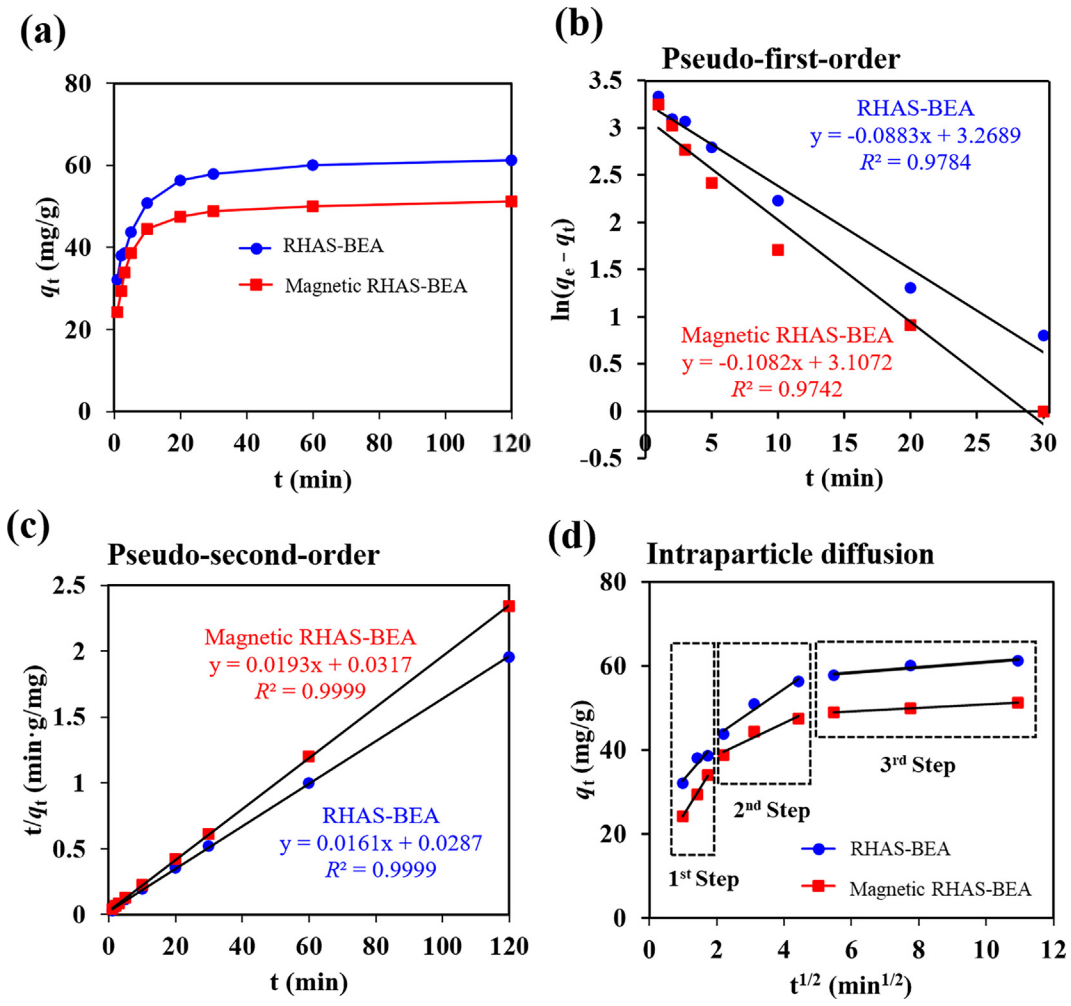

Fig. 6 (a) Change in amount of paraquat adsorbed on RHAS-BEA and magnetic RHAS-BEA over time and linear adsorption kinetic model plots including the (b) pseudo-first-order, (c) pseudo-second-order, and (d) intraparticle diffusion model. The initial concentration of paraquat was 75 mg/L, pH = 5.8 (non-adjusted).

multiple-step adsorption (Özacar, 2003); however, considering that the trend line did not pass through the origin in the first step (Fig. 6d), it was concluded that this was not the primary adsorption mechanism in this study. In conclusion, the overall rates of paraquat adsorption on both RHAS-BEA and magnetic RHAS-BEA may be controlled by a surface reaction step occurring through a chemisorption mechanism, as described by the pseudo-second-order model, rather than by the intraparticle diffusion step.

The results of the adsorption isotherm study (Fig. 7a) show an increase in the amount of adsorbed paraquat with increasing C_e which became saturated at approximately 70 and 50 mg/g for RHAS-BEA and magnetic RHAS-BEA, respectively. Two common linear adsorption isotherm models,

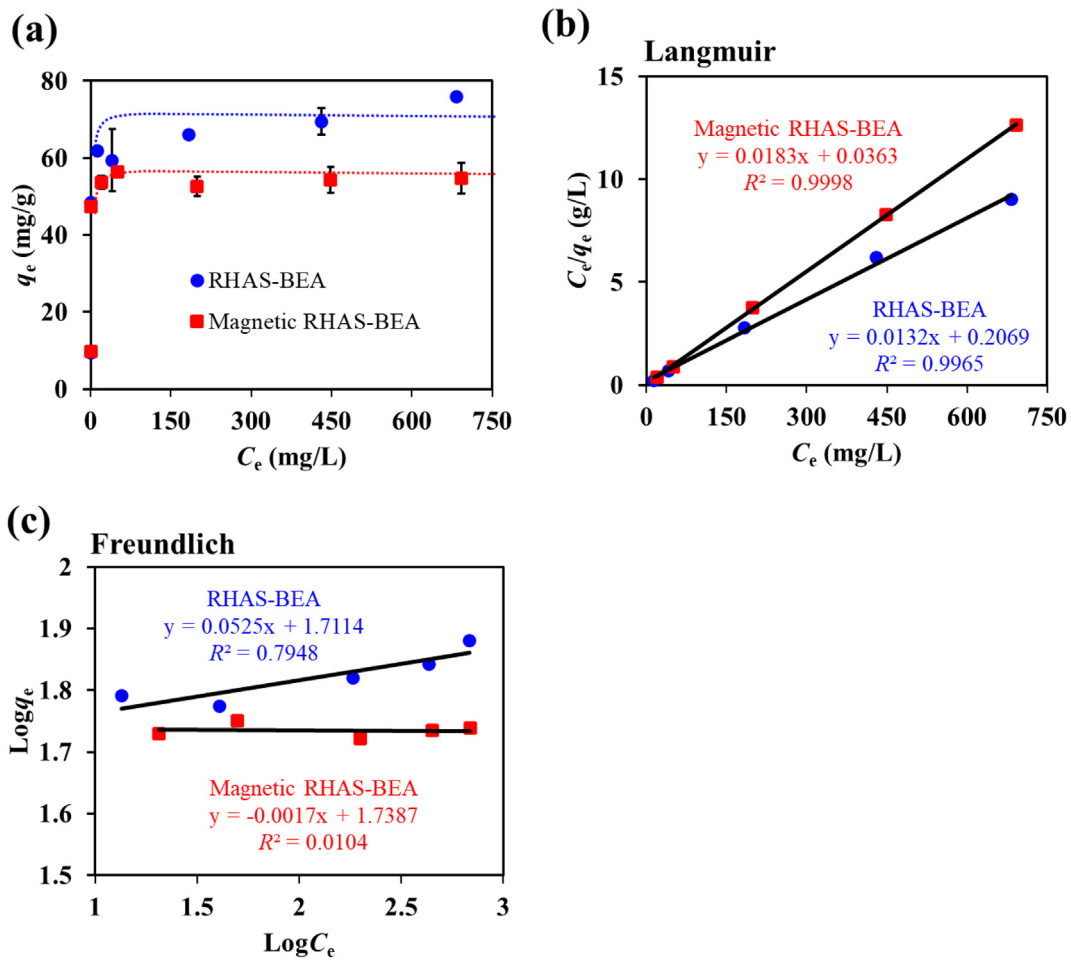

Fig. 7 (a) Adsorption isotherm of paraquat on RHAS-BEA and magnetic RHAS-BEA (error bars indicate the standard deviation), and a linear adsorption isotherm model plotted using (b) Langmuir and (c) Freundlich models. The initial concentration of paraquat was in the range 10–750 mg/L, pH = 5.8 (non-adjusted), contact time = 24 h. The experiments were carried out in duplicates.

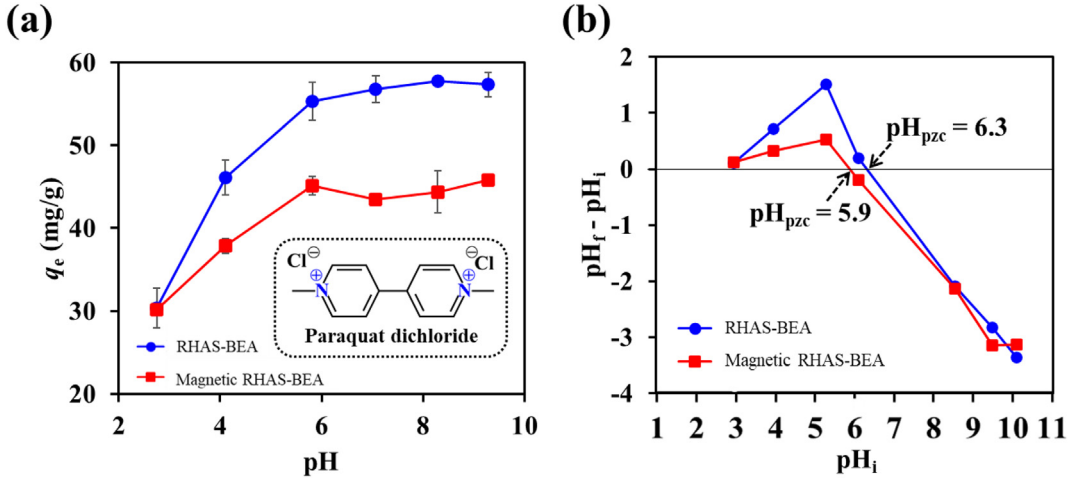

Fig. 8 (a) Effect of pH on the amount of paraquat adsorbed on RHAS-BEA and magnetic RHAS-BEA (error bars indicate the standard deviation of duplicate tests using the initial concentration of paraquat of 100 mg/L, contact time = 24 h), and (b) pH_{pzc} of the RHAS-BEA and magnetic RHAS-BEA.

namely, the Langmuir and Freundlich models, were used to explain the adsorption behavior. The Langmuir model was found to better describe the adsorption behavior of paraquat for both non-magnetic and magnetic RHAS-BEAs (Fig. 7b) than the Freundlich model (Fig. 7c). This model showed that paraquat is adsorbed as a monolayer on homogeneous adsorp-

tion sites on the surface of RHAS-BEA or magnetic RHAS-BEA (Rasaie et al., 2021). The Langmuir adsorption model was found to be the best fit for describing the adsorption of paraquat in zeolites (Insuwan and Rangsriwatananon, 2017; Keawkumay et al., 2019; Osakoo et al., 2017; Rongchapo et al., 2013; Rongchapo et al., 2015), mesoporous SiO_2 (Osakoo et al., 2017; Rasaie et al., 2021; Rongchapo et al., 2013, 2015), zeolite/mesoporous SiO_2 composites (Osakoo et al., 2017), graphene oxide/mesoporous SiO_2 composites (Dehghani et al., 2021), clays (Ait Sidhoum et al., 2013), and modified biopolymers (Fernandes et al., 2017; Huang et al., 2019a; Junthip et al., 2019). A plot based on the Langmuir model was used to determine the maximum adsorption amount of paraquat (q_m) of RHAS-BEA or magnetic RHAS-BEA to be 75.64 ± 1.09 and 54.71 ± 4.19 mg/g, respectively. Theoretically, the calculated BEA zeolite mass percentage in the calcined magnetic RHAS-BEA sample is approximately 72.6% (see Supplementary Information), which is believed to be the major contributor to paraquat adsorption. Because the maximum adsorption amount of magnetic RHAS-BEA was 72.3%, which is similar to 72.6%, the reason for the lower adsorption amount when using the magnetic sample was likely due to the fraction of iron oxide in the sample.

3.3. Effect of initial pH on paraquat adsorption and possible adsorption mechanism

In this study, the effect of the initial pH of the paraquat solution on adsorption capacity was investigated. The initial unadjusted pH of the tested paraquat solution was approximately 5.8, and we evaluated its adsorption amount in the pH range 3–9. pH values outside this range were not considered because: natural water is generally neutral; highly acidic conditions induce dealumination; and highly alkaline conditions trigger the dissolution of SiO_2. Overall, we found that the adsorption of paraquat onto the samples was pH-dependent in aqueous solutions. The results are shown in Fig. 8a. The q_e values were lower when the pH decreased from 5.8 to 3, but tended to increase when the pH was above 5.8, and plateauing once it went above 7. This trend was observed for both non-magnetic and magnetic RHAS-BEA samples. As shown in the paraquat structure (inset in Fig. 8a), no protons remained at the two positively charged quaternary amine groups (i.e., for further protonation or deprotonation), and its cationic form thus existed over a wide pH range. By determining the pH_{pzc}, we found that the pH variation greatly affected the surface charges on the adsorbents (Fig. 8b). Specifically, the pH_{pzc} values for RHAS-BEA and magnetic RHAS-BEA were 6.3 and

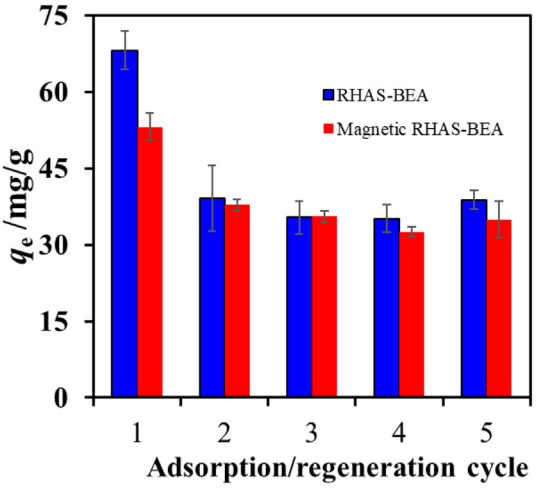

Fig. 10 Paraquat adsorption capacity of RHAS-BEA and magnetic RHAS-BEA after five consecutive adsorption/regeneration cycles. The tests were performed in duplicate for each cycle using the initial concentration of paraquat (500 mg/L), contact time = 24 h, and regeneration temperature = 450 °C (6 h).

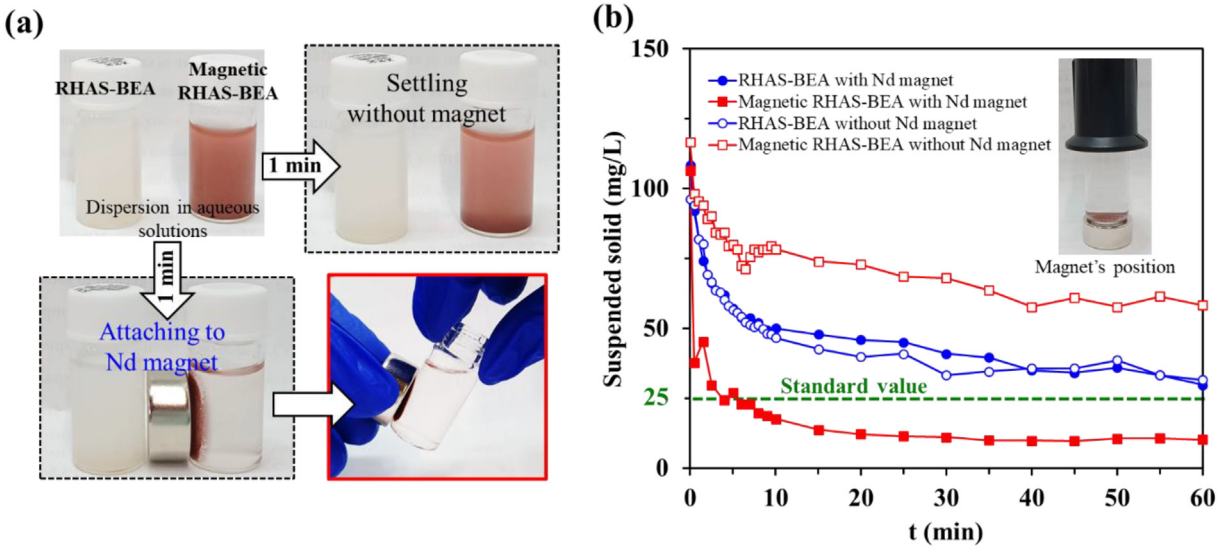

Fig. 9 (a) Separation of RHAS-BEA and magnetic RHAS-BEA suspension in aqueous solutions by settling the adsorbents without magnet and attaching to Nd magnet for 1 min, and (b) separability of the adsorbents by evaluating SS in the adsorbent suspension (100 mg/L) placing with Nd magnet (solid circle and square markers for RHAS-BEA and magnetic RHAS-BEA, respectively) and without Nd magnet (transparent circle and square markers for RHAS-BEA and magnetic RHAS-BEA, respectively).

Table 1 Maximum paraquat adsorption amount obtained from Langmuir model of the adsorbents in this study and previous studies.

Adsorbents	Adsorption test conditions					q_m (mg/g-adsorbent)	Reported number of reuses	Reference
	C_0 (mg/L)	Adsorbent dosage (g/L)	Contact time (min)	pH	Temperature (°C)			
k-carrageenan modified Fe_3O_4@SiO_2 nanosorbent	30–900	0.50	60	7.3	25	257	4 cycles*	Fernandes et al. (2017)
FAU (NaY) zeolite (Si/Al = 2.40)	100–1500	2.5	60	5	25	234.40	NR	Keawkumay et al. (2019)
FAU (NaY) zeolite (Si/Al = 3.5)	100–750	2.5	60	NR	RT	204.1	NR	Osakoo et al. (2017)
FAU (NaY) zeolite (Si/Al = 2.2)	80–1000	2.5	60	NR	RT	185.2	NR	Rongchapo et al. (2013)
K-LTL zeolite (Si/Al = 3.14)	50–500	2.0	1440	11	30	166.71	NR	Insuwan and Rangsriwatananon (2017)
FAU (NaY) zeolite /SBA-15 composite (Si/Al = 4.7)	100–750	2.5	60	NR	RT	144.9	NR	Osakoo et al. (2017)
BEA zeolite (Si/Al = 14.2)	80–1000	2.5	60	NR	RT	122.0	NR	Rongchapo et al. (2013)
FAU (NaX) zeolite (Si/Al = 1.27)	80–720	2.5	60	NR	RT	120.3	NR	Rongchapo et al. (2015)
Poly (vinyl alcohol)-cyclodextrin nanosponges	25–300	2	180	6.5	30	112.2	5 cycles*	Martwong et al. (2021)
2,2,6,6-tetramethylpiperidine 1-oxyl oxidized cellulose nanofibers	n.r.	0.10	120	7	30	108	NR	Huang et al. (2019a)
Algerian bentonite	50–300	2.0	1440	NR	25	100	NR	Ait Sidhoum et al. (2013)
FAU (HY) zeolite (Si/Al = 50)	50–250	1.0	1440	11	30	92.59	NR	Pukcothanung et al. (2018)
RHAS-BEA zeolite (Si/Al = 48.8)	10–750	1.0	1440	5.8	26	75.64	4 cycles	This study
SDS-modified FAU (HY) zeolite (Si/Al = 50)	50–250	1.0	1440	11	30	71.42	NR	Pukcothanung et al. (2018)
25%Al-MCM-41	80–560	2.5	60	NR	RT	65.6	NR	Rongchapo et al. (2015)
Magnetic RHAS-BEA zeolite (Si/Al = 45.0)	10–750	1.0	1440	5.8	26	54.71	4 cycles	This study
Graphene oxide/SiO_2	4–24	0.40	2	7	25	31.34	4 cycles	Dehghani et al. (2021)
H_LTL zeolite (Si/Al = 5.10)	50–500	2.0	1440	11	30	25.67	NR	Insuwan and Rangsriwatananon (2017)
Polyester textile coated with cyclodextrin	10–250	2	420	6.5	30	24.2	6 cycles*	Junthip et al. (2019)
MCM-41	80–1000	2.5	60	NR	RT	21.3	NR	Rongchapo et al. (2013)
Rice husk ash-SiO_2	80–1000	2.5	60	NR	RT	18.9	NR	Rongchapo et al. (2013)
Ketoenol–pyrazole receptor functionalized SiO_2	NR	2	NR	11.0	25 ± 0.1	17.63	5 cycles*	Jodeh et al. (2019)
SBA-3-SO_3H decorated Fe_3O_4/SiO_2 core shell nanoparticles	5–75	2.4	60	7.0	RT	14.73	6 cycles*	Kouchakinejad et al. (2022)
Bentonite/SiO_2	4–24	1.6	2	7	NR	11.75	NR	Rasaie et al. (2021)
Acid activated bentonite	4–24	1.6	2	NR	NR	5.93	NR	Rasaie et al. (2021)

NR = not reported; RT = Room temperature; * = number of reuses with no significant change in adsorption performance, including the first use.

5.9, respectively. At pH values below these points, the adsorbent surface charge is positive mainly because of the protonation of the hydroxyl groups (Mokrzycki et al., 2022), which electrostatically repel the positively charged amine of paraquat. Therefore, the values of q_e were lower in this pH region. Conversely, hydroxyl groups are deprotonated at pH values above the pH_{pzc}, generating negative charges on the adsorbent surface, which promote electrostatic interactions with the paraquat cation in addition to cation exchange at the alumina sites on the BEA zeolite framework. These contributions increased the q_e values. According to the pH results, paraquat adsorption can be improved through an increase of the initial pH. In this study, the q_m values were evaluated through adsorption isotherm studies, which were performed using the non-adjusted initial pH of the paraquat solutions (pH ≈ 5.8). However, the use of RHA-BEA and magnetic RHA-BEA at this pH provided sufficient paraquat adsorption and complied with the typical pH range for most natural waters (Pukcothanung et al., 2018).

At pH ≈ pH_{pzc}, the surface charge becomes zero; however, but greater q_e values than those in the lower pH region. Hence, interactions other than the aforementioned electrostatic forces may contribute to the adsorption mechanism. The paraquat molecule is smaller than size of the NaBEA zeolite cavity (Rongchapo et al., 2013), allowing it to be easily adsorbed via pore diffusion. Thus, cation exchange between cationic paraquat and Na^+ at the aluminum sites is thought to be the main mechanism by which adsorption occurs (Osakoo et al., 2017; Rongchapo et al., 2018) in this region. Several studies have reported the adsorption mechanism of paraquat using similar adsorbents. Hydrogen bonding also occurred during the adsorption of paraquat on mesoporous SiO_2-modified bentonite (Rasaie et al., 2021), and was found between the H atom of paraquat and the O atom centered around Al in the FAU zeolite (Keawkumay et al., 2019). Using X-ray photoelectron spectroscopy, Osakoo et al. showed that the binding energy between the C and N atoms of paraquat and the centered O atom in an FAU zeolite/mesoporous SiO_2 composite (Osakoo et al., 2017). The aromatic rings and methyl groups of paraquat also interact with the FAU zeolite framework (Rongchapo et al., 2018). These interactions supported the possible mechanism of action of paraquat on RHAS-BEA and magnetic RHAS-BEA synthesized by DGC.

3.4. Separability of the adsorbents from aqueous solutions

Fig. 9a illustrates the separation of the adsorbent particles from aqueous solutions with and without Nd magnets. In the absence of a magnet, both RHAS-BEA and magnetic RHAS-BEA samples slowly settled to the bottom of the containers, and most of the suspension remained in the liquid phase. When the Nd magnet was attached to the side of the containers, the magnetic sample quickly became attracted the magnetic field, resulting in a much clearer liquid phase after 1 min, whereas the non-magnetic sample did not react. Additionally, we checked the change in the concentration of SS in the liquid phase over 60 min (Fig. 9b). We found that the concentration of SS slowly decreased in the absence of a magnetic field for both samples. In the absence of a magnetic field, the magnetic sample sedimented more slowly because of its smaller particle size. However, when a magnetic field was applied, a slow decrease in SS was still observed for the RHAS-BEA sample because it was not being attracted by the magnet. In contrast, the SS sharply decreased in the magnetic RHAS-BEA sample to a concentration lower than that of the other samples, meeting the SS standard value for rivers set by the Japan Environmental Quality Standards for Protecting the Living Environment. These results indicate that the magnetic separability of the magnetic RHAS-BEA sample was not affected by the co-existing α-Fe_2O_3, that is, the weakly magnetic phase. Therefore, the inclusion of Fe_3O_4 in the RHA-BEA zeolite greatly facilitated the collection of adsorbents after the removal of paraquat.

3.5. Reusability and ions leached from the adsorbents during adsorption

In addition to adsorption performance and magnetic separability, economic feasibility was considered (i.e., in terms of

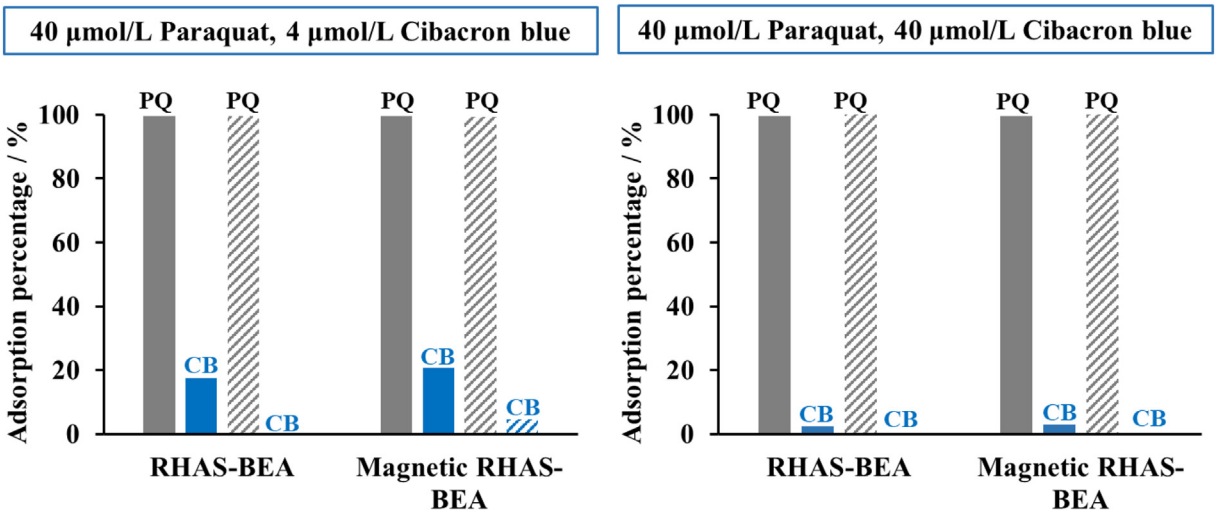

Fig. 11 Paraquat (PQ) removal efficiency of RHAS-BEA and magnetic RHAS-BEA tested in single (solid-fill bars) and binary (pattern-fill bars) systems.

reusability). This is an important aspect when considering the applicability of a water treatment approach. In most studies, the adsorption of paraquat on adsorbents is mainly ion-exchange, which is inhibited in acidic media or at high salinity. Several studies have reported that paraquat can be desorbed from adsorbents using salts (Ait Sidhoum et al., 2013) or acidic solutions (Dehghani et al., 2021; Jodeh et al., 2019; Kouchakinejad et al., 2022). In this study, we focused on waste handling after adsorbent regeneration. Hence, thermal treatment of the spent adsorbents was considered to remove the adsorbed paraquat. Pure paraquat thermally decomposes at 300 °C (Haley, 1979), thus the adsorbents were recalcined in air at 450 °C after paraquat adsorption. The q_e values for RHAS-BEA and magnetic RHAS-BEA obtained from the first recalcination cycle decreased by approximately 40% and 30%, respectively, compared to those of the pristine samples. However, these samples remained unchanged for three additional re-adsorption cycles (Fig. 10). The lower adsorption performance after the first cycle can be attributed to the incomplete removal of adsorbed paraquat under the applied recalcination conditions. The thermal decomposition residue may remain the least accessible adsorption site, hindering the access of paraquat molecules in the second cycle and cycles thereafter. Regardless of their initial use, the adsorbents could be reused for at least four cycles without showing degradation in their performance. Given the advantages of using recycled agricultural waste, high conversion rate of the DGC method, and magnetic separability, the adsorption capacities of the reused RHAS-BEA and magnetic RHAS-BEA (37.08 ± 7.95 and 35.21 ± 4.04 mg/g, respectively) are still acceptable because they are maintained at levels comparable to those of several types of fresh adsorbents, as shown in Table 1. The adsorption

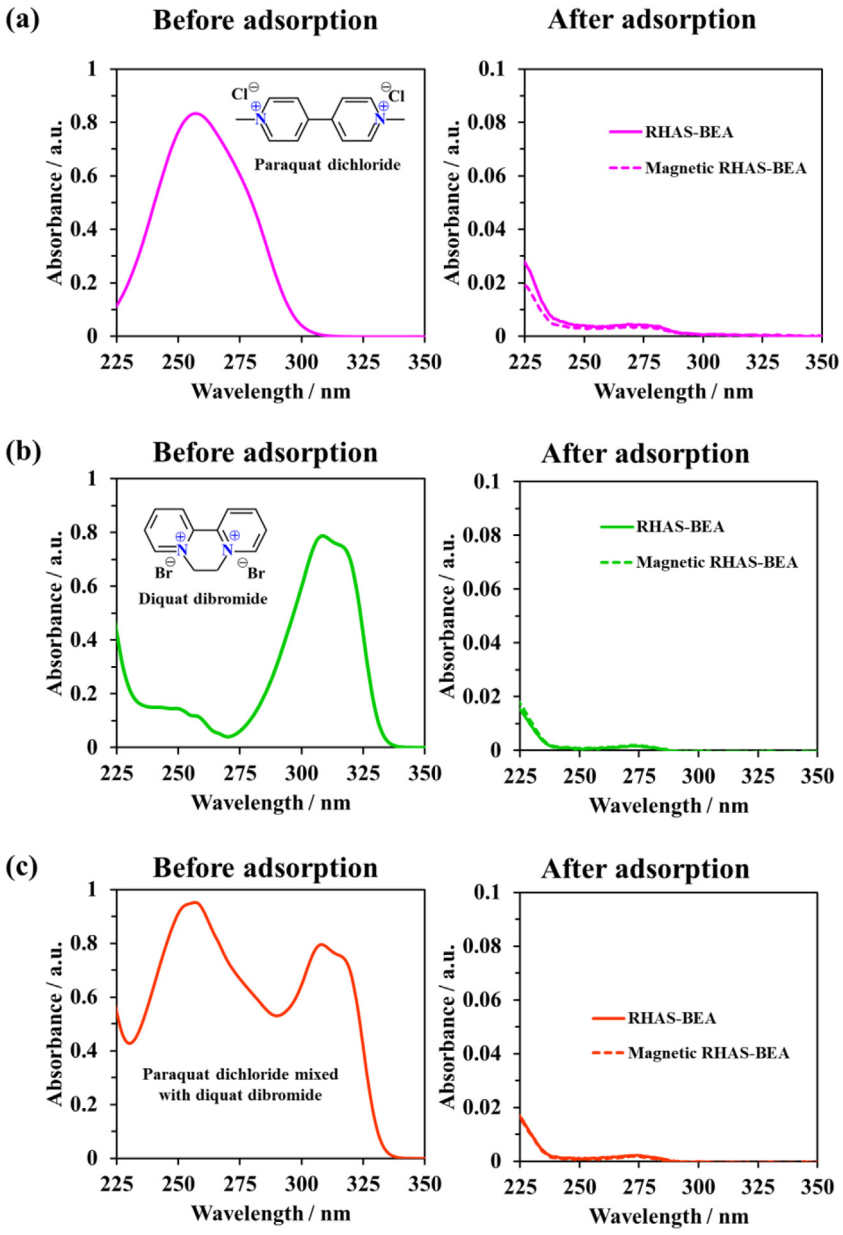

Fig. 12 UV absorption spectra of (a) paraquat and (b) diquat before and after single adsorption tests, and (c) paraquat and diquat before and after binary adsorption test.

performance of the non-magnetic and magnetic RHAS-BEA samples among the four reuses emphasizes that the inclusion of Fe_3O_4 particles in the BEA zeolite does not negatively impact adsorption.

For the ion-leaching test, Si was found to slightly leach from the adsorbents while Al was not detected in the solutions during the 3-h shaking time at pH ≈ 6. The detected level of Si for RHAS and magnetic RHAS adsorbent in the solutions were 1 mg/L and 0.4 mg/L, respectively, which were approximately 0.1 wt% and 0.04 wt% of the pristine RHAS and magnetic RHAS adsorbents, respectively. The negligible leaching of Si indicates that the developed adsorbents are stable under the tested conditions. For the magnetic RHAS adsorbent, Fe leaching was not detected during the adsorption test, which also supports the idea that the magnetic particles were incorporated inside the zeolite particles.

3.6. Paraquat co-adsorption with blue dye

The results of paraquat adsorption using the developed adsorbents in the presence of CB are shown in Fig. 11. Our adsorbents showed a paraquat removal efficiency of more than 99% in the presence of CB, a representative blue dye commonly added to commercial herbicides to avoid accidental poisoning (Nur et al., 2005; Rongchapo et al., 2013). The presence of blue dye at both concentrations did not suppress the adsorption of paraquat, whereas the adsorbents only adsorbed a small amount of CB since its molecular size is much larger than paraquat. This implies that the developed adsorbent enables the selective removal of paraquat from commercial herbicides.

3.7. Paraquat co-adsorption with diquat

Herbicides with similar structures to paraquat might also be adsorbed using the developed adsorbents through similar mechanism. Diquat, not only the similarity in structure (Fig. 12), is one of the commonly used herbicides together with paraquat (Ronnen et al., 1995) and has negative effect to human health (Uematsu et al., 2021). Thus, both paraquat and diquat should be removed from water. The results in Fig. 12a and b show the decreasing in UV absorption intensity of the solutions after single adsorption tests to below the detection limit of the spectrophotometer for both paraquat and diquat using RHAS-BEA and magnetic RHAS-BEA. This indicates that diquat is also adsorbed onto the developed adsorbents. In binary adsorption test result (Fig. 12c), no strong UV absorption bands were detected for both paraquat and diquat after adsorption. Therefore, the RHAS-BEA and magnetic RHAS-BEA are also applicable for removal of those two herbicides.

3.8. Adsorption performance comparison with other types of adsorbents

Direct comparison of the adsorption performance among various types of adsorbents is difficult owing to variations in the experimental conditions and nature of a respective adsorbent. The maximum adsorption amounts obtained from the Langmuir model for the adsorbents in this study and from previous reports are summarized in Table 1. Our adsorbents showed higher q_m values than those of several types of adsorbents, such as mesoporous SiO_2, clays, graphene oxide, and H-LTL zeolites, but lower adsorption performance than the low-SiO_2 zeolites reported in several papers, including the BEA zeolite prepared by conventional hydrothermal synthesis using RHAS (Rongchapo et al., 2013). However, the advantages of our adsorbents are as follows: they can be easily collected through magnetic separation; they are created through the use of agricultural waste–derived ingredients; and they can also be reused. Furthermore, our adsorbents exhibited a paraquat-removal efficiency of more than 99% in the presence of blue dye. Hence, RHAS-BEA and magnetic RHAS-BEA could be used as alternative candidates for paraquat removal from contaminated waters.

4. Conclusion

This paper presents the sustainable utilization of bulky solid RHAS in the synthesis of magnetic BEA zeolites for herbicide removal using the DGC method. The utilization of solid-state RHAS in the preparation of a uniform dry precursor gel is possible with the assistance of ultrasonic waves. Magnetic BEA zeolites were successfully obtained by using this protocol without any adverse effects from the incorporated Fe_3O_4 particles. The prepared sample was used for the removal of paraquat from aqueous solutions via an adsorption process, which was shown to have a high rate, quick magnetic separability, and excellent reusability for at least five cycles. This study contributes to sustainable circulation in agriculture because of the utilization of agricultural-waste–derived materials for remediating water polluted through agricultural activities. Overall, the approach presented in this study is environmentally friendly and cost-effective.

CRediT authorship contribution statement

Vanpaseuth Phouthavong: Data curation, Formal analysis, Investigation, Methodology, Visualization, Writing – original draft. **Takeshi Hagio:** Conceptualization, Investigation, Methodology, Project administration, Supervision, Writing – original draft. **Jae-Hyeok Park:** Investigation, Formal analysis, Writing – review & editing. **Supinya Nijpanich:** Validation, Writing – review & editing. **Teeranun Srihirunthanon:** Investigation, Formal analysis, Validation. **Nutchanan Chantanurak:** Investigation, Formal analysis, Validation. **Kanchanok Duangkhai:** Investigation, Formal analysis, Validation. **Ratana Rujiravanit:** Resources, Supervision, Writing – review & editing. **Vanseng Chounlamany:** Formal analysis, Writing – review & editing. **Kesiny Phomkeona:** Supervision, Writing – review & editing. **Long Kong:** Data curation, Visualization, Writing – review & editing. **Liang Li:** Data curation, Supervision, Writing – review & editing. **Ryoichi Ichino:** Funding acquisition, Supervision.

Declaration of Competing Interest

The authors declare that they have no known competing financial interests or personal relationships that could have appeared to influence the work reported in this paper.

Acknowledgements

The first author gratefully acknowledges a scholarship from the Yoshida Scholarship Foundation for his studies at Nagoya University, Japan.

Funding

This work received partial financial support from the Strategic International Collaborative Research Program (SICORP) [grant number JPMJSC18H1] of the Japan Science and Technology Agency and a research grant from the Kyosho Hatta Foundation, Japan. The authors also appreciate relational support from the National Key Research and Development Program of China (No. 2017YFE0127100).

Appendix A. Supplementary material

Supplementary data to this article can be found online at https://doi.org/10.1016/j.arabjc.2023.104959.

References

Ait Sidhoum, D., Socías-Viciana, M.M., Ureña-Amate, M.D., Derdour, A., González-Pradas, E., Debbagh-Boutarbouch, N., 2013. Removal of paraquat from water by an Algerian bentonite. Appl. Clay Sci. 83–84, 441–448. https://doi.org/10.1016/j.clay.2013.07.007.

Ardiwinata, A.N., Harsanti, E.S., Kurnia, A., Sulaeman, E., 2021. The distribution of paraquat and carbosulfan residues in Indonesia. IOP Conf. Ser.: Earth Environ. Sci. 648,. https://doi.org/10.1088/1755-1315/648/1/012033 012033.

Banerjee, S., Barman, S., Halder, G., 2017. Sorptive elucidation of rice husk ash derived synthetic zeolite towards deionization of coalmine waste water: a comparative study. Groundw. Sustain. Dev. 5, 137–151. https://doi.org/10.1016/j.gsd.2017.06.004.

Bok, T.O., Andriako, E.P., Knyazeva, E.E., Ivanova, I.I., 2020. Engineering of zeolite BEA crystal size and morphology via seed-directed steam assisted conversion. RSC Adv. 10, 38505–38514. https://doi.org/10.1039/D0RA07610D.

Criado, M., Fernández-Jiménez, A., de la Torre, A.G., Aranda, M.A. G., Palomo, A., 2007. An XRD study of the effect of the SiO_2/Na_2O ratio on the alkali activation of fly ash. Chem. Concr. Res. 37, 671–679. https://doi.org/10.1016/j.cemconres.2007.01.013.

Dang, L.V., Le, S.T., Lobo, R.F., Pham, T.D., 2020. Hydrothermal synthesis of alkali-free chabazite zeolites. J. Porous Mater. 27, 1481–1489. https://doi.org/10.1007/s10934-020-00923-y.

Dehghani, Z., Sedghi-Asl, M., Ghaedi, M., Sabzehmeidani, M.M., Adhami, E., 2021. Ultrasound-assisted adsorption of paraquat herbicide from aqueous solution by graphene oxide/mesoporous silica. J. Environ. Chem. Eng. 9,. https://doi.org/10.1016/j.jece.2021.105043 105043.

El Maksod, I.H.A., Al-Shehri, A., Bawaked, S., Mokhtar, M., Narasimharao, K., 2017. Structural and photocatalytic properties of precious metals modified TiO_2-BEA zeolite composites. Mol. Catal. 441, 140–149. https://doi.org/10.1016/j.mcat.2017.08.012.

FAO, 2022. Food and Agriculture Organization of the United Nations. https://www.fao.org/faostat/en/#data/QCL/visualize accessed date 13.10.2022

Fauzi, A., Ratnawulan, R., 2021. The effect of calcination temperature on the structure of iron oxide phase from west Sumatra. J. Phys. Conf. Ser. 1876,. https://doi.org/10.1088/1742-6596/1876/1/012028 012028.

Fernandes, T., Soares, S.F., Trindade, T., Daniel-da-Silva, A.L., 2017. Magnetic hybrid nanosorbents for the uptake of paraquat from water. Nanomaterials 7, 68. https://doi.org/10.3390/nano7030068.

Flores, C.G., Schneider, H., Dornelles, J.S., Gomes, L.B., Marcilio, N. R., Melo, P.J., 2021. Synthesis of potassium zeolite from rice husk ash as a silicon source. Cleaner Eng. Technol. 4,. https://doi.org/10.1016/j.clet.2021.100201 100201.

Franco, D.S.P., Georgin, J., Lima, E.C., Silva, L.F.O., 2022. Advances made in removing paraquat herbicide by adsorption technology: a review. J. Water Process Eng. 49,. https://doi.org/10.1016/j.jwpe.2022.102988 102988.

Gebretatios, A.G., Kadiri Kanakka Pillantakath, A.R., Witoon, T., Lim, J.W., Banat, F., Cheng, C.K., 2023. Rice husk waste into various template-engineered mesoporous silica materials for different applications: A comprehensive review on recent developments. Chemosphere. 310, 136843. https://doi.org/10.1016/j.chemosphere.2022.136843

Hagio, T., Nijpanich, S., Kunishi, H., Yamaoka, K., Phouthavong, V., Kamimoto, Y., Ichino, R., Iwai, K., 2019. Synthesis of MOR zeolite/magnetite composite via seed assisted method. J. Nanosci. Nanotechnol. 19, 6841–6848. https://doi.org/10.1166/jnn.2019.17123.

Haley, T.J., 1979. Review of the toxicology of paraquat (1,1′-dimethyl-4,4′-bipyridinium chloride). Clin. Toxicol. 14, 1–46. https://doi.org/10.3109/15563657909030112.

Huang, C.F., Tu, C.W., Lee, R.H., Yang, C.H., Hung, W.C., Andrew Lin, K.Y., 2019a. Study of various diameter and functionality of TEMPO-oxidized cellulose nanofibers on paraquat adsorptions. Polym. Degrad. Stab. 161, 206–212. https://doi.org/10.1016/j.polymdegradstab.2019.01.023.

Huang, Y., Zhan, H., Bhatt, P., Chen, S., 2019b. Paraquat degradation from contaminated environments: current achievements and perspectives. Front. Microbiol. 10, 1754. https://doi.org/10.3389/fmicb.2019.01754.

Inagaki, S., Nakatsuyama, K., Saka, Y., Kikuchi, E., Kohara, S., Matsukata, M., 2007. Elucidation of medium-range structure in a dry gel-forming *BEA-type zeolite. J. Phys. Chem. C 111, 10285–10293. https://doi.org/10.1021/jp0668044.

Insuwan, W., Rangsriwatananon, K., 2017. Removal of paraquat from aqueous solutions onto zeolite LTL. Eng. J. 21, 15–23. https://doi.org/10.4186/ej.2017.21.2.15.

Jiao, Y., Han, D., Lu, Y., Rong, Y., Fang, L., Liu, Y., Han, R., 2017. Characterization of pine-sawdust pyrolytic char activated by phosphoric acid through microwave irradiation and adsorption property toward CDNB in batch mode. Desalinization Water Treat. 77, 247–255. https://doi.org/10.5004/dwt.2017.20780.

Jodeh, S., Hanbali, G., Tighadouini, S., Radi, S., Hamed, O., Jodeh, D., 2019. Removal and extraction efficiency of Quaternary ammonium herbicides paraquat (PQ) from aqueous solution by ketoenol–pyrazole receptor functionalized silica hybrid adsorbent (SiNPz). BMC Chem. 13, 86. https://doi.org/10.1186/s13065-019-0599-2.

Junthip, J., Jumrernsuk, N., Klongklaw, P., Promma, W., Sonsupap, S., 2019. Removal of paraquat herbicide from water by textile coated with anionic cyclodextrin polymer. SN Appl. Sci. 1, 106. https://doi.org/10.1007/s42452-018-0102-z.

Keawkumay, C., Rongchapo, W., Sosa, N., Suthirakun, S., Koleva, I. Z., Aleksandrov, H.A., Vayssilov, G.N., Wittayakun, J., 2019. Paraquat adsorption on NaY zeolite at various Si/Al ratios: a combined experimental and computational study. Mater. Chem. Phys. 238,. https://doi.org/10.1016/j.matchemphys.2019.121824 121824.

Kouchakinejad, R., Shariati, S., Abolhasani, J., Kalhor, E.G., Vardini, M.T., 2022. Core-shells of magnetite nanoparticles decorated by SBA-3-SO_3H mesoporous silica for magnetic solid phase adsorption of paraquat herbicide from aqueous solutions. Colloids Surf. A Physicochem. Eng. Asp. 643,. https://doi.org/10.1016/j.colsurfa.2022.128709 128709.

Li, J., Gao, M., Yan, W., Yu, J., 2023. Regulation of the Si/Al ratios and Al distributions of zeolites and their impact on properties. Chem. Sci. 14, 1935–1959. https://doi.org/10.1039/D2SC06010H.

Loiola, A.R., Bessa, R.A., Oliveira, C.P., Freitas, A.D.L., Soares, S. A., Bohn, F., Pergher, S.B.C., 2022. Magnetic zeolite composites: Classification, synthesis routes, and technological applications. J.

Magn. Magn. Mater. 560,. https://doi.org/10.1016/j.jmmm.2022.169651 169651.
Martwong, E., Chuetor, S., Junthip, J., 2021. Adsorption of paraquat by poly(vinyl alcohol)-cyclodextrin nanosponges. Polymers 13, 4110. https://doi.org/10.3390/polym13234110.
Matsukata, M., Osaki, T., Ogura, M., Kikuchi, E., 2002. Crystallization behavior of zeolite beta during steam-assisted crystallization of dry gel. Micropor. Mesopor. Mater. 56, 1–10. https://doi.org/10.1016/S1387-1811(02)00412-2.
Miao, S., She, P., Chang, X., Zhao, C., Sun, Y., Lei, Z., Sun, S., Zhang, W., Jia, M., 2022. Synthesis of beta nanozeolite aggregates with hierarchical pores via steam-assisted conversion of dry gel and their catalytic properties for Friedel-Crafts acylation. Micropor. Mesopor. Mater. 334,. https://doi.org/10.1016/j.micromeso.2022.111777 111777.
Mokrzycki, J., Fedyna, M., Marzec, M., Szerement, J., Panek, R., Klimek, A., Bajda, T., Mierzwa-Hersztek, M., 2022. Copper ion-exchanged zeolite X from fly ash as an efficient adsorbent of phosphate ions from aqueous solutions. J. Environ. Chem. Eng. 10,. https://doi.org/10.1016/j.jece.2022.108567 108567.
Moradi, S.E., 2014. Microwave assisted preparation of sodium dodecyl sulphate (SDS) modified ordered nanoporous carbon and its adsorption for MB dye. J. Ind. Eng. Chem. 20, 208–215. https://doi.org/10.1016/j.jiec.2013.04.005.
Nur, H., Manan, A.F.N., Wei, L.K., Muhid, M.N.M., Hamdan, H., 2005. Simultaneous adsorption of a mixture of paraquat and dye by NaY zeolite covered with alkylsilane. J. Hazard. Mater. 117, 35–40. https://doi.org/10.1016/j.jhazmat.2004.07.015.
Osakoo, N., Pansakdanon, C., Sosa, N., Deekamwong, K., Keawkumay, C., Rongchapo, W., Chanlek, N., Jitcharoen, J., Prayoonpokarach, S., Wittayakun, J., 2017. Characterization and comprehension of zeolite NaY/mesoporous SBA-15 composite as adsorbent for paraquat. Mater. Chem. Phys. 193, 470–476. https://doi.org/10.1016/j.matchemphys.2017.03.002.
Özacar, M., 2003. Equilibrium and kinetic modelling of adsorption of phosphorus on calcined alunite. Adsorption 9, 125–132. https://doi.org/10.1023/A:1024289209583.
Phouthavong, V., Hiraiwa, M., Hagio, T., Nijpanich, S., Chounlamany, V., Nishihama, T., Kamimoto, Y., Ichino, R., 2020. Magnetic BEA-type zeolites: Preparation by dry-gel conversion method and assessment of dye removal performance. J. Mater. Cycles Waste Manag. 22, 375–382. https://doi.org/10.1007/s10163-020-00994-8.
Prasetyoko, D., Ramli, Z., Endud, S., Hamdan, H., Sulikowski, B., 2006. Conversion of rice husk ash to zeolite beta. Waste Manag. 26, 1173–1179. https://doi.org/10.1016/j.wasman.2005.09.009.
Pukcothanung, Y., Siritanon, T., Rangsriwatananon, K., 2018. The efficiency of zeolite Y and surfactant-modified zeolite Y for removal of 2,4-dichlorophenoxyacetic acid and 1,1′-dimethyl-4,4′-bipyridinium ion. Micropor. Mesopor. Mater. 258, 131–140. https://doi.org/10.1016/j.micromeso.2017.08.035.
Rasaie, A., Sabzehmeidani, M.M., Ghaedi, M., Ghane-Jahromi, M., Sedaratian-Jahromi, A., 2021. Removal of herbicide paraquat from aqueous solutions by bentonite modified with mesoporous silica. Mater. Chem. Phys. 262,. https://doi.org/10.1016/j.matchemphys.2021.124296 124296.
Rongchapo, W., Sophiphun, O., Rintramee, K., Prayoonpokarach, S., Wittayakun, J., 2013. Paraquat adsorption on porous materials synthesized from rice husk silica. Water Sci. Technol. 68, 863–869. https://doi.org/10.2166/wst.2013.311.
Rongchapo, W., Deekamwong, K., Loiha, S., Prayoonpokarach, S., Wittayakun, J., 2015. Paraquat adsorption on NaX and Al-MCM-41. Water Sci. Technol. 71, 1347–1353. https://doi.org/10.2166/wst.2015.100.
Rongchapo, W., Keawkumay, C., Osakoo, N., Deekamwong, K., Chanlek, N., Prayoonpokarach, S., Wittayakun, J., 2018. Comprehension of paraquat adsorption on faujasite zeolite X and Y in sodium form. Adsorpt. Sci. Technol. 36, 684–693. https://doi.org/10.1177/0263617417715394.
Ronnen, M., Klin, B., Suster, S., 1995. Mixed diquat/paraquat-induced burns. Int. J. Dermatol. 34, 23–25. https://doi.org/10.1111/j.1365-4362.1995.tb04371.x.
Saleh, I.A., Zouari, N., Al-Ghouti, M.A., 2020. Removal of pesticides from water and wastewater: chemical, physical and biological treatment approaches. Environ. Technol. Innov. 19,. https://doi.org/10.1016/j.eti.2020.101026 101026.
Santana Costa, J.A.S., Paranhos, C.M., 2018. Systematic evaluation of amorphous silica production from rice husk ashes. J. Clean. Prod. 192, 688–697. https://doi.org/10.1016/j.jclepro.2018.05.028.
Shams, T., Schober, G., Heinz, D., Seifert, S., 2022. Rice husk ash as a silica source for the production of autoclaved aerated concrete – a chance to save energy and primary resources. J. Build. Eng. 57,. https://doi.org/10.1016/j.jobe.2022.104810 104810.
Sivalingam, S., Sen, S., 2020. Rice husk ash derived nanocrystalline ZSM-5 for highly efficient removal of a toxic textile dye. J. Mater. Res. Technol. 9, 14853–14864. https://doi.org/10.1016/j.jmrt.2020.10.074.
Steven, S., Restiawaty, E., Bindar, Y., 2021. Routes for energy and bio-silica production from rice husk: a comprehensive review and emerging prospect. Renew. Sustain. Energ. Rev. 149,. https://doi.org/10.1016/j.rser.2021.111329 111329.
Tan, K.L., Hameed, B.H., 2017. Insight into the adsorption kinetics models for the removal of contaminants from aqueous solutions. J. Taiwan Inst. Chem. Eng. 74, 25–48. https://doi.org/10.1016/j.jtice.2017.01.024.
Tolentino, C.M.C., de Luna, M.D.G., Futalan, C.M., Choi, A.E.S., Manegdeg, F.G., Grisdanurak, N., 2020. Influence of hydrocarbons on hydrogen chloride removal from refinery off-gas by zeolite NaY derived from rice husks. Sci. Total Environ. 728,. https://doi.org/10.1016/j.scitotenv.2020.138782 138782.
Uematsu, Y., Ogata, F., Nagai, N., Saenjum, C., Nakamura, T., Kawasaki, N., 2021. In vitro removal of paraquat and diquat from aqueous media using raw and calcined basil seed. Heliyon 7, e07644.
Walcarius, A., Mouchotte, R., 2004. Efficient in vitro paraquat removal via irreversible immobilization into zeolite particles. Arch. Environ. Contam. Toxicol. 46, 135–140. https://doi.org/10.1007/s00244-003-2242-3.
Wang, Y., Du, T., Jia, H., Qiu, Z., Song, Y., 2018. Synthesis, characterization and CO2 adsorption of NaA, NaX and NaZSM-5 from rice husk ash. Solid State Sci. 86, 24–33. https://doi.org/10.1016/j.solidstatesciences.2018.10.003.